

## The Behaviour of Tribocorrosion on EH47 High-Strength Ship Hull Steel in a 3.5% NaCl Solution

Hongmei Zhang<sup>1,2,\*</sup>, Yan Li<sup>2</sup>, Na Li<sup>1</sup>, Ling Yan<sup>2</sup>, Yangyang Zhu<sup>1</sup>, Changshun Wang<sup>2</sup>,  
Fangfang Ai<sup>2</sup>, Zhengyi Jiang<sup>1,3\*</sup>

<sup>1</sup> School of Material and Metallurgy, University of Science and Technology Liaoning, Anshan 114051, China

<sup>2</sup> State Key Laboratory of Metal Material for Marine Equipment and Application, Liaoning, Anshan, 114009

<sup>3</sup> School of Mechanical, Materials and Mechatronic Engineering, University of Wollongong, Wollongong NSW 2522, Australia

\*E-mail: [zhanghm@ustl.edu.cn](mailto:zhanghm@ustl.edu.cn), [jiang@uow.edu.au](mailto:jiang@uow.edu.au)

Received: 6 August 2019 / Accepted: 29 September 2019 / Published: 29 October 2019

---

In this paper, the tribocorrosion behaviour of EH 47 high-strength ship hull steel in a 3.5% NaCl solution was investigated. The tribological and corrosion tests were carried out on a Si<sub>3</sub>N<sub>4</sub> ball-on-EH47 high-strength ship hull steel disc tribometer under different sliding time conditions. The disks were continuously immersed in sandy 3.5% NaCl solution during the whole process of the tribological tests. After the tribological tests, electrochemical tests were carried out to obtain typical polarization curves and electrochemical impedance spectroscopy diagrams. The corrosion experiments were performed to investigate the effect of abrasion on corrosion behaviour by immersing the samples in a container with 3.5% NaCl solution and 5 wt.% silica sand at room temperature for 7, 14, and 49 days. The micrographs, compositions and corrosion products of the worn scars were evaluated by scanning electron microscopy (SEM) and energy dispersive spectroscopy (EDS) microanalyses.

---

**Keywords:** Corrosion; Abrasion; Marine environment; Wear mechanism; Tribological tests

### 1. INTRODUCTION

At present, the development and utilization of marine resources have become a hot issue in the world, and the market demand for marine equipment and engineering steel is great [1,2]. Corrosion is a harmful process to ships that can lead to fatigue cracking, brittle fracture and structural degradation caused by ageing. These failures can mean the risk of loss of life and pollution of the environment[3, 4]. Due to poor service conditions, marine equipment and marine engineering, steel needs to withstand long-term continuous wave impact and seawater erosion. The corrosion problem of marine engineering

materials causes a large amount of the energy wasted by marine vehicles every year and has become one of the technical bottlenecks restricting the development of major marine engineering technologies and equipment. Therefore, the corrosion and failure mechanisms of materials have become an urgent problem to be solved in the field of marine engineering [5, 6].

Since the 1930s, a large number of studies on the corrosion of materials in natural seawater have been carried out by scholars of industrially developed countries such as the United States and Europe. The United States has published 16 years of corrosion data for 52 materials and 3 years of corrosion data for 475 materials [7]. Wang et al. [8, 9] proposed the off-site corrosion behaviour evaluation technique for evaluating environmental behaviour by electrochemical methods and databases of 5 kinds of ocean engineering steel that is used at depths of 5000 metres. Al-Muhanna et al. [10] investigated the influence of season and temperature change on the metal corrosion behaviour in the Kuwait channel using an electrochemical impedance technique. Quej-Aké et al. [11] reported the corrosion inhibition effect of non-ionic surfactant on X52 pipeline steel in NaCl solution. Gao et al. [12] studied the initial corrosion behaviour of X80 pipeline steel in yellow sea water. Melchers [13] presented long-term immersion corrosion on steel in seawater with a relatively high nutrient concentration in the seawater. Toloel et al. [14] investigated the synergistic effect of seawater parameters under the corrosion rate of carbon steel, including pH value, temperature and salinity in a turbulent state. Zhang et al. [15] studied the influence of tempering temperature on corrosion behaviour of R5 steel in artificial seawater. Zhou et al. [16] reported the corrosion behaviour of low-carbon micro-alloyed steel in a Cl-containing environment. Shen et al. [17] studied the corrosion behaviour of EH40 steel in a low-temperature NaCl solution. Melchers [18] proposed a detailed report of steel corrosion and models to explain the various corrosion mechanisms. Zayed et al. [19] and Panayotova et al. [20] described the main environmental factors that affect the main corrosion mechanisms.

In the corrosive medium of a harsh marine environment, a layer of surface film with properties different from the matrix will be formed on the metal surface [21]. This film will be thinned or broken or experience other complex changes due to friction or particle impact [22]. Wear can thin or damage the passivation film, exposing the surface to the solution. Agitation of the solution accelerates the diffusion of corrosion products (metal ions), and the surface shear force increases surface dislocations, vacancies and other defects; the above results increase the surface activity that leads to corrosion acceleration, and the corrosion rate of the metal is thus increased [23-26]. Analyses of corrosion and wear of 304SS stainless steel and the interaction between corrosion and wear show that the friction and wear process promote the occurrence of macroscopic electrical corrosion of materials and intensify the corrosion tendency of materials [27]. Papageorgiou et al. [28] presented his work on tribocorrosion mechanisms of a NiCrMo-625 alloy.

After corrosion, the surface of the material or the rust layer on the surface is loose and porous, and it is easily washed away by friction or particles in the process of abrasion, which increases the material loss and roughness of the metal surface and aggravates the wear [29-31]. Under oceanic conditions, the surface of carbon steel generally cannot form a stable film of blunt corrosion products but rather forms a loose rust layer. This film provides little protection against further corrosion. In the process of abrasion, the rust film on the surface of the material is quickly scraped away under the

action of abrasion, resulting in the failure to form a complete protective film in the worn area, thus showing an interaction between corrosion and wear [31-33].

Due to outstanding low-temperature impact toughness, high strength, prominent weldability, and high-performance ship plate steel extensions, the high-strength EH47 grade ship steel exhibits great potential for polar expedition ships. To investigate the tribocorrosion behaviour of the EH47 high-strength ship hull steel in 3.5% NaCl solution, tribological and corrosion tests were carried out on a Si<sub>3</sub>N<sub>4</sub> ball-on-EH47 high-strength ship hull steel disc tribometer for 240 min, 120 min, and 60 min at loads of 100 N. The disks were continuously immersed in sandy 3.5% NaCl solution during the whole process of the tribological tests. After the tribological tests, electrochemical tests were carried out by a CHI760E electrochemical workstation using a working electrode with corrosion samples under different wear conditions and an electrolyte with seawater at room temperature. The corrosion experiments were carried out by immersing the samples in a container at room temperature for 14 and 49 days after the wear test.

## 2. EXPERIMENTAL

### 2.1 Materials

EH47 was used as the disk material in this study and is a low-alloyed high-strength ship hull steel. The chemical composition of the disk material is (in wt.%) C: 0.07, Si: 0.20, Mn: 1.42, P: 0.006, S: 0.001, Cr: 0.07, Ni: 0.79, Mo: 0.22, Nb: 0.04, V: 0.006, Ti:0.013, Al: 0.03 and Fe balance.

### 2.2 Experimental tests

The wear tests were performed by an Rtec MFT-5000 Multi-functional Tribometer under different sliding time conditions. The disks were immersed in a 3.5% NaCl solution with 5% sand at 0 °C (salt water with ice).

### 2.3 Electrochemical measurement

All electrochemical tests were carried out in seawater at room temperature. The test samples were EH47 steel under different wear conditions (distinguished by numbers). The samples were first cleaned with deionized water, then ultrasonically cleaned with ethanol and dried in a dryer. After wrapping the copper wire with an insulating skin at one end of the non-corroded surface of the sample and evenly applying an epoxy resin on the non-test surface with a brush, the grooved part of the sample (the test surface) was set aside as the area of the working electrode. All electrochemical tests were carried out using a three-electrode system with a platinum sheet electrode as the auxiliary electrode, a saturated calomel electrode as the reference electrode, the corrosion samples under different environmental wear conditions as the working electrodes, and room-temperature seawater as the electrolyte. The electrochemical measurements were performed using a CHI760E electrochemical workstation produced by Shanghai ChenHua Instrument Co., Ltd. The scanning speed of the

polarization curve test was 0.5 mV/s, and the scanning range was -200~200 mV relative to the open circuit potential. The frequency range of the electrochemical ac impedance was 0.1 ~ 10 MHz, and the voltage amplitude was 10 mV.

#### 2.4 Corrosion Experiment

After the wear experiments, the corrosion experiments were carried out for 7, 14, and 49 days by immersing the samples in a container at room temperature. The container was filled with 3.5% NaCl solution and 5 wt.% silica sand.

#### 2.5 Characterization methods

The 3D profile of worn tracks on the disks was observed by a Keyence VK-5000 3D Laser Scanning Microscope. The micrographs and surface composition of the abrasion scar surfaces and the corrosion surface were performed by a scanning electron microscope (ZEISS-Sigma, SEM, German) and with energy dispersive spectroscopy (EDS) microanalyses.

### 3. RESULTS AND DISCUSSION

#### 3.1 Wear test

The wear tests were performed by the Rtec MFT-5000 Multi-functional Tribometer under different sliding time conditions. The disks were immersed in salt water with ice and sand throughout the entire test. The SEM micrograph of worn scars on the disk surface under different sliding times is shown in Fig. 1. It can be observed that the worn scars on the disk surface are deeper along the sliding direction with increasing sliding time. The micro-voids and abrasion scars are more evident and larger under 240 min and 120 min sliding times than under a 60 min sliding time, as shown in the SEM image in Fig. 1(a), (b), (c), and (d). Meanwhile, the wear track scratches on the worn surface have great differences with the sliding time of 60 min. It is noted that the worn disk tracks of 120 min sliding are also severely ploughed, while the micro-voids and adhesive areas are much more abundant at 120 min than at 60 min. In particular, the worn disk surface appears to have a slight abrasion, and there are fewer pits and micro-voids on the worn disk with a 60 min sliding time than with other sliding times, as shown in Fig. 1(e) and (f). The presence of ploughing grooves on the worn surface in the direction of sliding is a dominant feature exhibited in Fig. 1(b), (d), and (e). The primary mechanism is abrasion due to the action of sand particles, while ploughing dominates the whole abrading process and leads to high friction and wear for the ball on the test disk under a high-loading force. Meanwhile, the micro-voids and isolated pits indicate that surface fatigue plays a great role on the wear of the disk[34]. Therefore, the wear mechanisms are an abrasive-wear mechanism and a fatigue-wear mechanism at relatively high loadings and sliding times of 240 min and 120 min, as shown in Fig. 1(a), (b), (c), and (d). It should be noted that there is an adhesive effect between the disk surface and ball that has a slight influence on the wear mechanism.

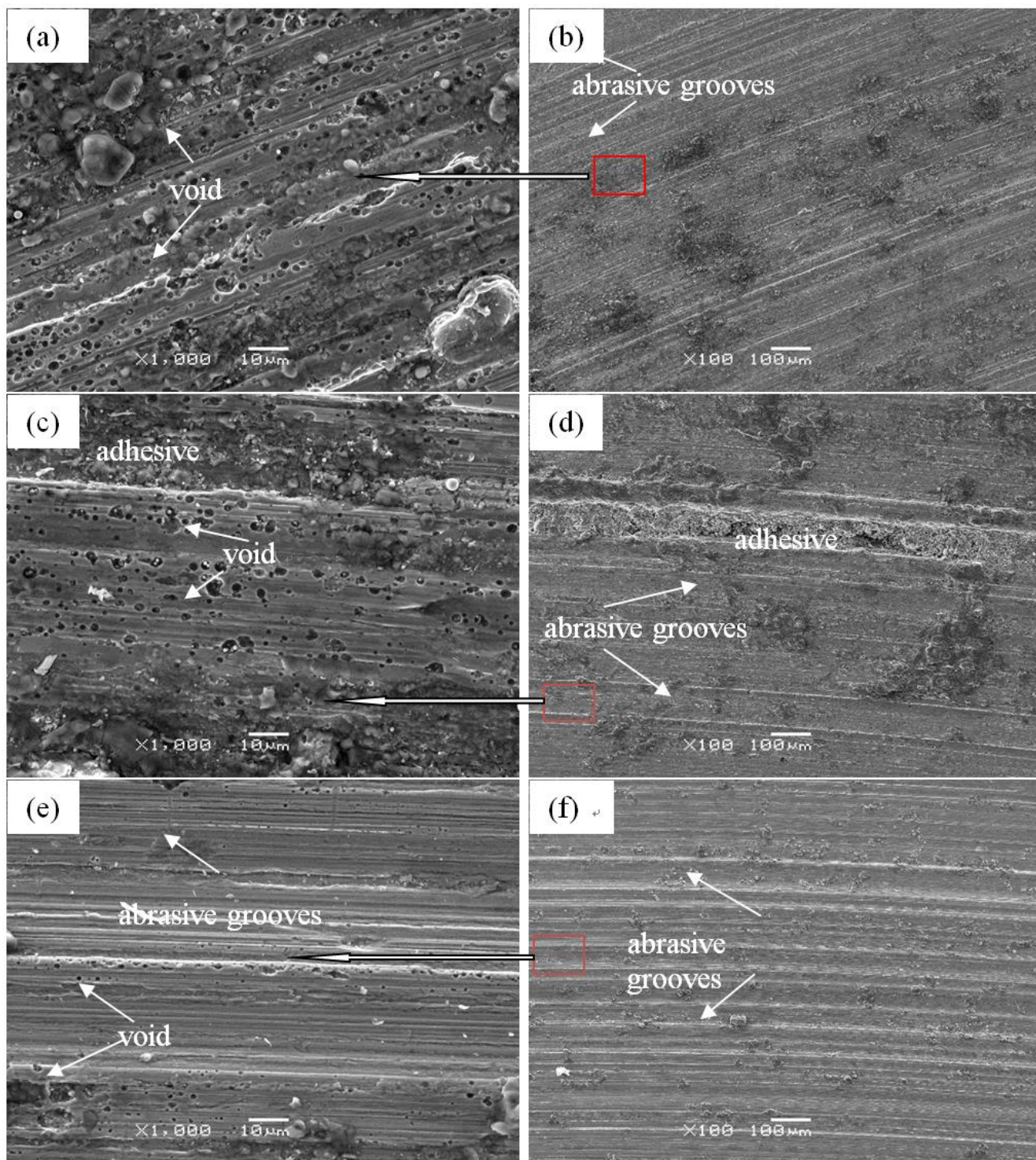


**Figure 1.** SEM micrographs of worn scars on the disk surface under different sliding conditions (100 N loads, 200 rpm sliding rate, disks immersed in 3.5% salt water with ice and sand):(a) (b) sliding time of 240 min, (c) (d) sliding time of 120 min, and (e) (f) sliding time of 60 min.

### 3.2 Potentiodynamic polarization curve analysis

All electrochemical tests were carried out in seawater at room temperature. The test samples were EH47 steel under different wear conditions (distinguished by numbers).

The electrochemical corrosion process can be analysed with polarization curve measurements. The electrochemical fitting parameters, i.e., corrosion current densities ( $I_{\text{corr}}$ ), corrosion potential ( $E_{\text{corr}}$ ), polarization resistance ( $R_p$ ), and anodic and cathodic Tafel constants ( $\beta_a$ ,  $\beta_c$ ), were obtained by extrapolation of Tafel lines[35, 36]. The typical polarization curves of the studied steel in salt water for 0 days after different sliding times of 240 min, 120 min, 60 min and 0 min are shown in Fig. 2. The fitting data are shown in Table 1. As shown in Table 1, the corrosion current density of the original sample is lower than that of samples of all sliding times, which indicates that the wear will accelerate the corrosion. Meanwhile, the corrosion current density of the 120 min sliding time is lower than that of the 60 min and 240 min sliding times, indicating that the corrosion rate does not increase with the sliding time. The smallest corrosion rate is observed at 120 min, and the largest corrosion rate is observed at 60 min. From the polarization curves, it can also be seen that the cathodic and anodic reaction rate shapes of the curves did not change greatly with increasing sliding time, which indicates that the wear process did not significantly affect the cathodic and anodic reaction processes. The change trends of the largest corrosion potential ( $E_{\text{corr}}$ ) and polarization resistance are the opposite of each other: the smallest corrosion potential ( $E_{\text{corr}}$ ) and largest polarization resistance appear at 120 min, and the largest corrosion potential and smallest polarization resistance are obtained at 60 min. The results show that the corrosion current densities obtained under tribocorrosion conditions are higher than those obtained under corrosion-only conditions. Friction obviously accelerates the corrosion of the samples.

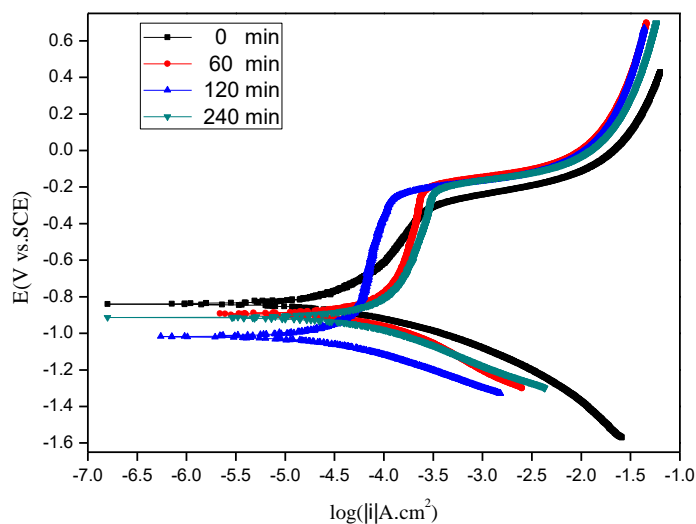


**Figure 2.** Polarization curves of EH47 steel (the samples were obtained after the wear test under different sliding times of 0 min, 60 min, 120 min, and 240 min with 100 N loads and a 200 rpm sliding rate).

The typical polarization curves of the studied sample with different sliding times and immersion in salt water for 14 days are shown in Fig. 3. The fitting data are shown in Table 2. From the polarization curves, the cathodic and anodic reaction rate shapes of the curves show little change with sliding time and corrosion time, which indicated that the wear process had little effect on the cathodic and anodic reaction processes. The Tafel slope constants ( $\beta_a$  and  $\beta_c$ ) do not change significantly

in the inhibited system compared to the uninhibited system. This suggests that the inhibitor does not participate in the mechanism of corrosion [36,37]. The corrosion current density for the 0 min sliding time is lower than that for all other sliding times, indicating that wear can accelerate corrosion, as shown in Table 2. Furthermore, the corrosion current density of the 120 min sliding time is also lower than that of the 60 min sliding time, which indicates that the corrosion rate does not increase with sliding time. The smallest corrosion rate is observed at 120 min, and the largest corrosion potential is observed at 240 min. The change trends of the largest corrosion potential ( $E_{corr}$ ) and polarization resistance are the opposite of each other, with the smallest corrosion potential ( $E_{corr}$ ) and largest polarization resistance appearing at 120 min and the largest corrosion potential ( $E_{corr}$ ) and smallest polarization resistance appearing at 0 min. The results show that the corrosion current densities obtained under tribocorrosion conditions after 14 days of corrosion are higher than those under corrosion-only conditions and under tribocorrosion conditions after 0 days of corrosion. The increasing corrosion time and friction can obviously accelerate the corrosion of the samples.

**Table 1.** Potentiodynamic polarization parameters from applying a curve-fitting approach to EH47 steel data (the samples were obtained after the wear test under different sliding times of 0 min, 60 min, 120 min, and 240 min with 100 N loads and a 200 rpm sliding rate).

Sliding time (min)	$E_{corr}$ (V. SCE <sup>-1</sup> )	$I_{corr}$ (A.cm <sup>-2</sup> )	$R_p$ (Ω.cm <sup>2</sup> )
0	-0.84	$2.19 \times 10^{-5}$	1651
60	-0.89	$5.93 \times 10^{-5}$	791
120	-1.02	$2.36 \times 10^{-5}$	1772
240	-0.91	$5.48 \times 10^{-5}$	819

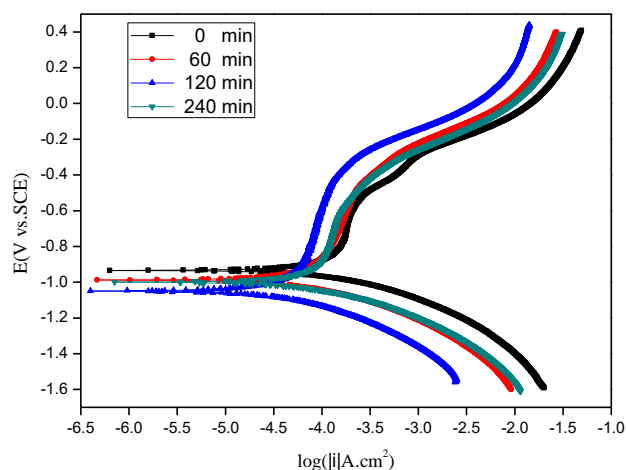


**Figure 3.** Polarization curves of EH47 steel . The samples were obtained after the wear test under different sliding times of 0 min, 60 min, 120 min, and 240 min with 100 N loads, a 200 rpm sliding rate and immersion in 3.5% NaCl solution for 14 days.

**Table 2.** Potentiodynamic polarization parameters from a curve-fitting approach under different sliding times of 0 min, 60 min, 120 min, and 240 min (the samples were obtained after the wear test under different sliding times with 100 N loads, a 200 rpm sliding rate and immersion in 3.5% salt water for 14 days).

Sliding time (min)	$E_{corr}$ (V. SCE <sup>-1</sup> )	$I_{corr}$ (A.cm <sup>-2</sup> )	$R_p$ (Ω.cm <sup>2</sup> )
0	-0.93	11.07	408
60	-0.98	6.55	677
120	-1.05	3.52	1286
240	-1.00	7.70	564

### 3.3 Electrochemical impedance spectroscopy

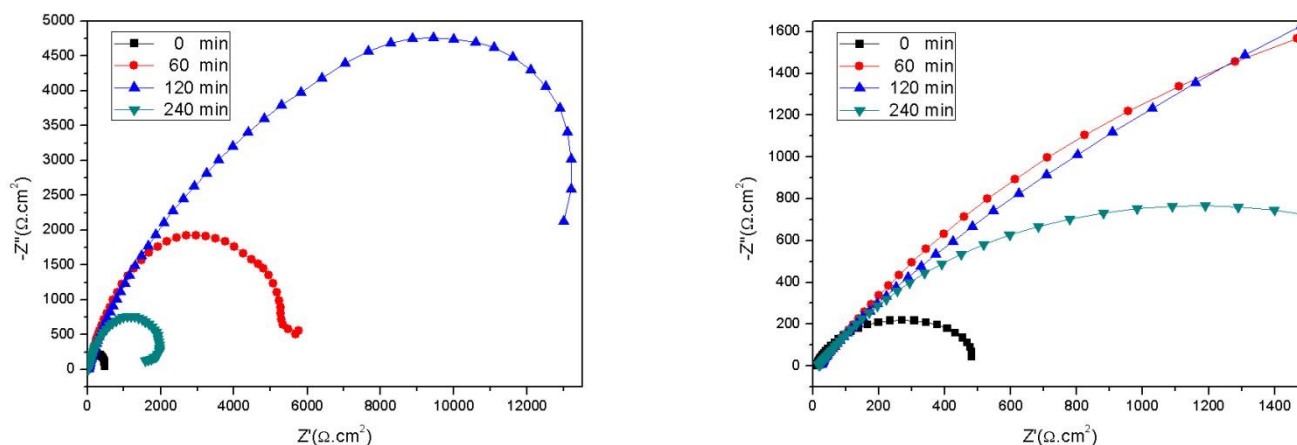


**Figure 4.** EIS of EH47 steel at different sliding times of 0 min, 60 min, 120 min, and 240 min (the samples were obtained after the wear test under different sliding times with 100 N loads and a 200 rpm sliding rate).

EIS has been employed frequently in determining the kinetics of metals and alloys for electron transfer reactions at the metal/solution interface [38,39]. The electrochemical impedance spectroscopy (EIS) curves of the studied steel at different sliding times of 240 min, 120 min, 60 min and 0 min are shown in Fig. 4. In Fig. 4, each Nyquist plot shows a single capacitive loop in the measured range of applied frequency. The capacitive loops at high frequency reflect the electrochemical impedance characteristics of a film and the double electron layer on the metal surface [40], and the inductive loops at low frequency are attributed to the occurrence of pitting corrosion or the adsorption relaxation process of some species. [41]. The impedance response behaviour of EH47 steel shows significant changes at different sliding times of 240 min, 120 min, 60 min and 0 min. The largest reactance arc of EIS in the low-frequency region occurs at the 120 min sliding time, and the smallest radius of the capacitive reactance arc is at the 0 min sliding time. It was reported that capacitive loops reflect the EIS

behaviour of a surface film and double electron layer on the surface of metals and alloys [22]. In the present study, the presence of a single capacitive loop is attributed to a surface passive film on EH47. As the radius of the capacitive reactance arc decreases, the transfer resistance on the surface of the alloy decreases, which reflects decreased corrosion resistance.

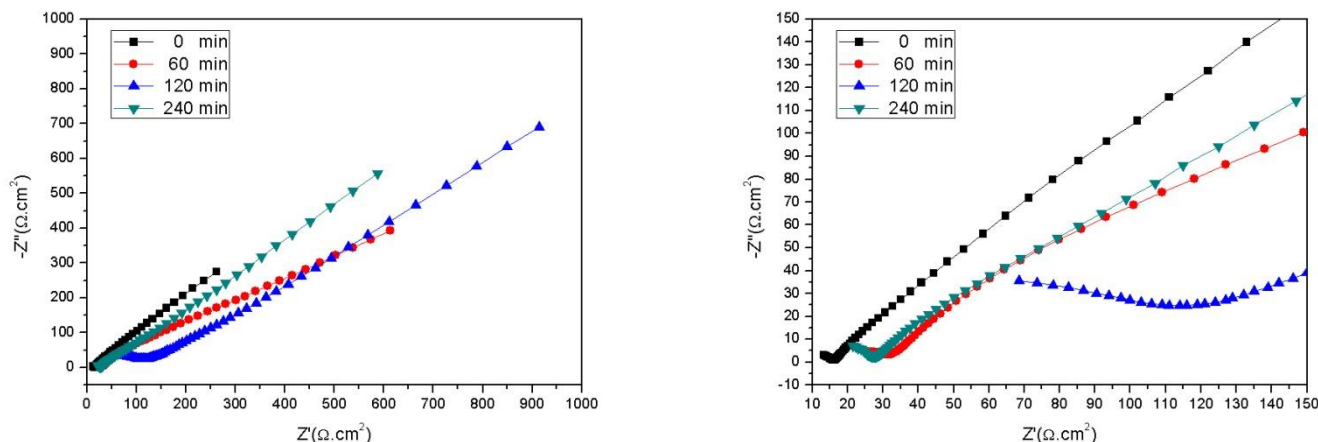


**Figure 5.** EIS of EH47 steel at different sliding times of 0 min, 60 min, 120 min, and 240 min (the samples were obtained after the wear test under different sliding times with 100 N loads, a 200 rpm sliding rate, and immersion in 3.5% NaCl solution for 14 days)

In previous studies, much research has been conducted on the synergistic effect of the erosion-corrosion effect[42]. Guo and Lu[43] investigated the interaction of mechanical and electrochemical factors in the erosion-corrosion process of A1045 carbon steel. Gao investigated the cavitation erosion-corrosion process of Q235 and ZG06Cr13Ni4Mo with various applied potentials [44].

The electrochemical impedance spectroscopy (EIS) curves of the studied steel immersed in a container with 3.5% NaCl solution for 14 days at different sliding times of 240 min, 120 min, 60 min and 0 min are shown in Fig. 5. The impedance response behaviour of EH47 steel shows a very small change at different sliding times of 240 min, 120 min, 60 min and 0 min. Each Nyquist plot shows a single capacitive loop in the measured range of applied frequency from Fig. 5. The reactance arc of EIS in the low-frequency region is very different at the different sliding times of 240 min, 120 min, 60 min and 0 min. Compared with the EIS results of Fig. 4, these EIS results are different. Furthermore, the largest reactance arc of EIS in the low-frequency region occurs at the 0 min sliding time, and the smallest radius of the capacitive reactance arc occurs at the 120 min sliding time. The above EIS results indicate that the corrosion time has a significant influence on the corrosion rate. The capacitance and reactance arc in the low-frequency region reflects the transfer process of charge or material through the corrosion product layer. As the capacitance and reactance arc radius decrease, the transfer resistance on the surface of the alloy decreases, and the corrosion resistance of the alloy is reduced. That is, the sliding time and corrosion have an influence on the corrosion rate; on the other hand, abrasion can accelerate the corrosion.

## 3.4 Corrosion product analysis

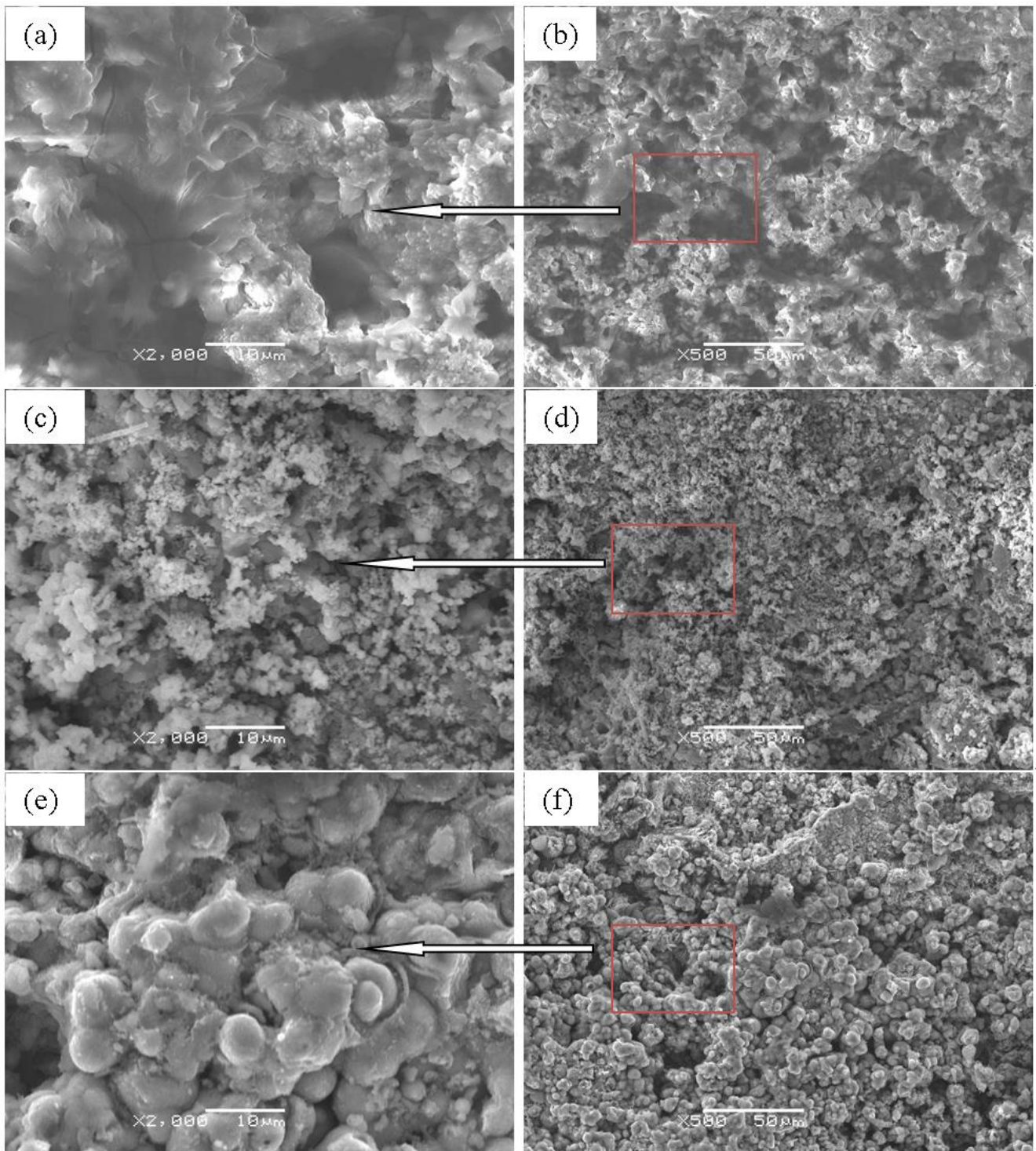


**Figure 6.** Disk surface corrosion layer morphology of the worn track: (a) (b) 60 min, (c) (d) 120 min, and (e) (f) 240 min (the samples were obtained after the wear test under different sliding times with 100 N loads, a 200 rpm sliding rate, and immersion in 3.5% NaCl solution for 7 days).

Fig. 6 indicates the corrosion morphology of the worn track on the disk surface after immersion in 3.5% NaCl solution after 7 days. The corrosion product on the surface of the disk is not very dense

and has microcracks, as shown in Fig. 6. There are two types of micrographs for the corrosion product on the worn tracks of the disk.

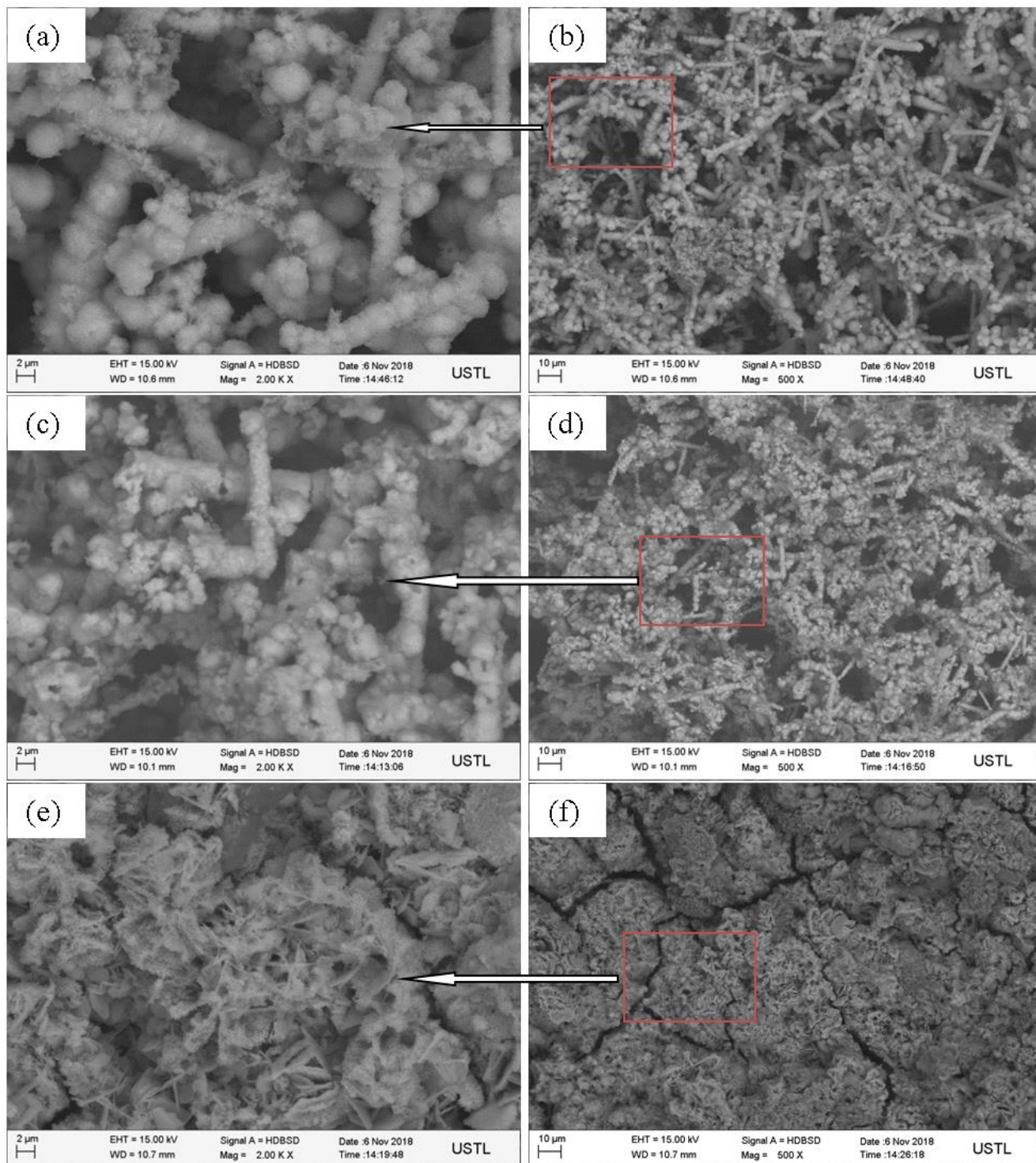


**Figure 7.** Disk surface corrosion layer morphology of the worn track: (a) (b) 60 min, (c) (d) 120 min, and (e) (f) 240 min (the samples were obtained after the wear test under different sliding times with 100 N loads, a 200 rpm sliding rate, and immersion in 3.5% NaCl solution for 14 days).

The one type presents a block shape that gradually agglomerated, as shown in Fig. 6 (a), (b), (c), and (d). The other is a cluster structure of the corrosion product, as shown in Fig. 6 (e) and (f). Hence, at long sliding times, the corrosion product on the wear tracks of the disk is denser and has fewer microcracks than that at short sliding times.

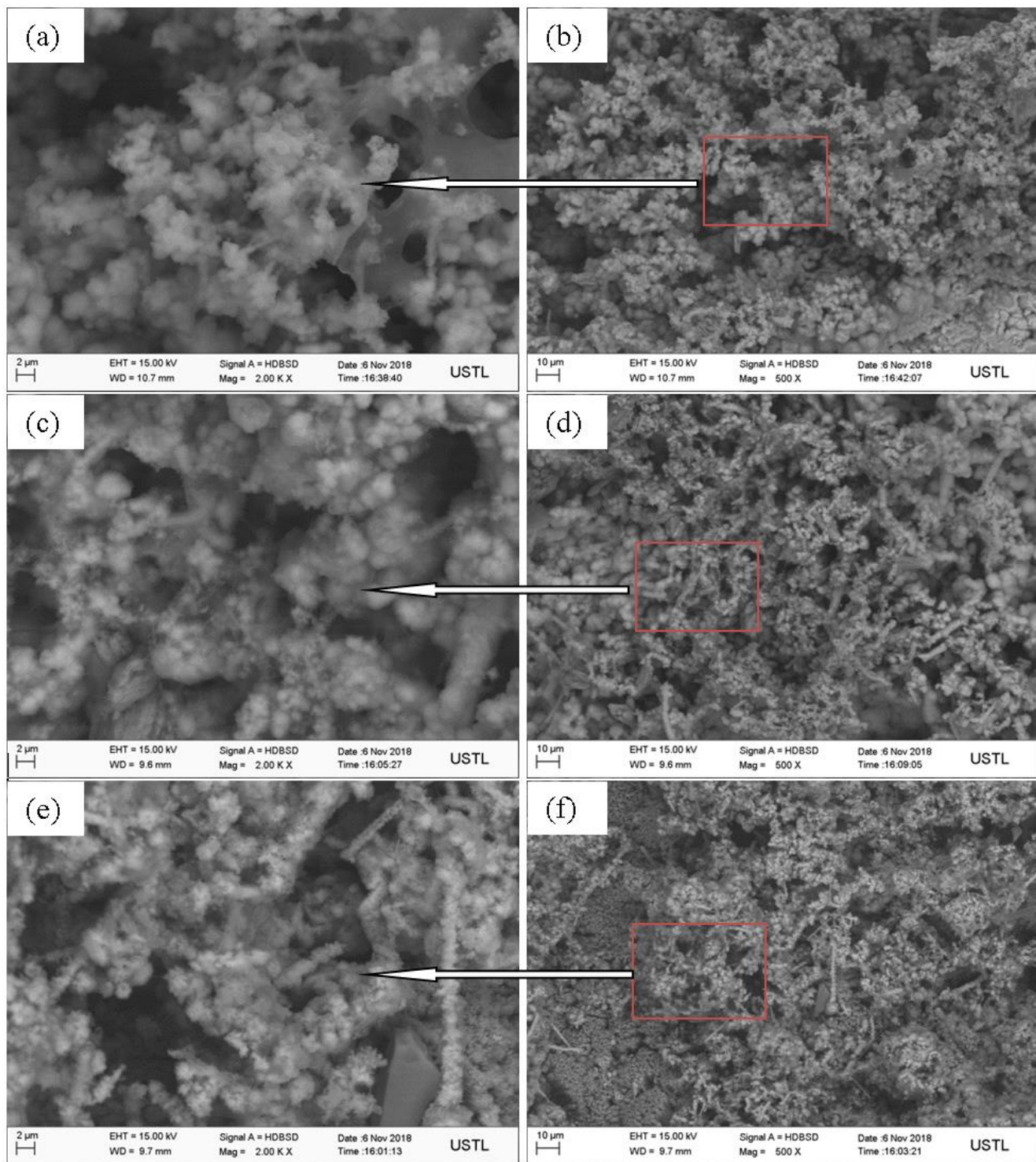


**Figure 8.** Disk surface corrosion layer morphology of the worn track: (a) (b) 60 min, (c) (d) 120 min, and (e) (f) 240 min (the samples were obtained after the wear test under different sliding times with 100 N loads, a 200 rpm sliding rate, and immersion in 3.5% NaCl solution for 49 days).

Fig. 7 presents a micrograph of the corrosion layer on the worn tracks of the disk after 14 days of immersion in 3.5% NaCl solution. It can be clearly observed from Fig. 7 that the rust layer corrosion on the worn tracks of the disk has a needle cluster structure, and there are many microcracks. The corrosion product layers have flower-like shapes with increasing sliding time, as shown in Fig. 7 (e) and (f). The corrosion product on the worn tracks of the 14 day disk is denser than that of the 7 day sample and presents the needle cluster structure. This indicates that the layer is thick and cracked, which means that it may have pits underneath[45].

Fig. 8 presents a micrograph of the corrosion layer on the worn tracks of the disk after 49 days of immersion in 3.5% NaCl solution. It can be seen that the corrosion product on the worn tracks of this disk is denser than that of the 7 day and 14 day samples and presents a fine needle cluster structure. Shen et al. [17] described the corrosion behaviour of modified EH40 steel in a low-temperature (0 °C) 3.5 wt.% NaCl solution over a 56-day period. The compact and thick corrosion product film covered the steel surfaces that protected the steel from further corrosion, and a characteristic uniform corrosion was present in the steel.

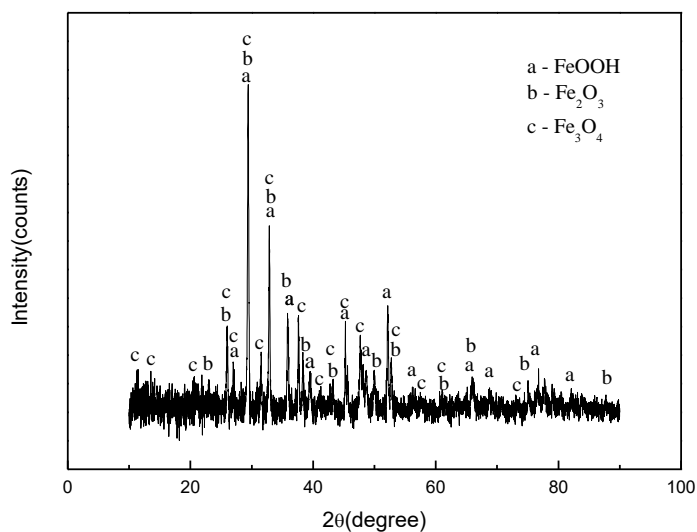


**Figure 9.** XRD of the disk surface corrosion layer of the worn track after 30 days immersion in 3.5% NaCl solution.

Fig. 9 presents the XRD results of the corrosion layer on the worn track immersed in 3.5% NaCl solution after 30 days. The corrosion products formed on the samples are a series of complex reaction products of FeOOH, Fe<sub>2</sub>O<sub>3</sub>, and Fe<sub>3</sub>O<sub>4</sub>, as shown in Fig. 9.

Fig. 10 shows that the corrosion product film is mainly composed of Fe, C and O elements. Among them, due to the loose and weak film structure of the corrosion products, part of the Fe matrix components are included in the scanning process, so a strong Fe peak appears in the EDS spectrum.

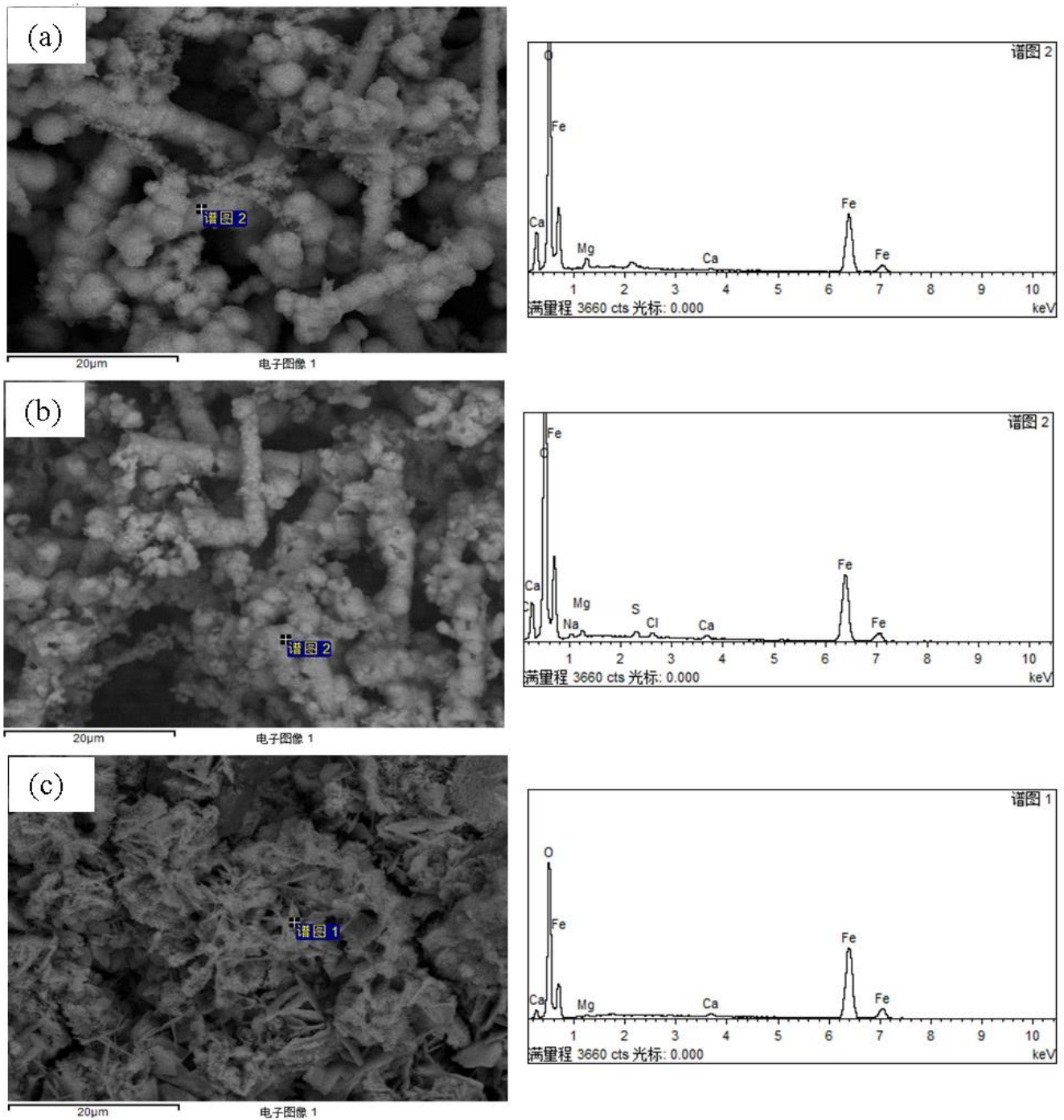


**Figure 10.** EDS of the corrosion products on the worn track: (a) 60 min, (b) 120 min, and (c) 240 min (the samples were obtained after the wear test under different sliding times with 100 N loads, a 200 rpm sliding rate, and immersion in 3.5% NaCl solution for 14 days).

#### 4. CONCLUSIONS

(1) It is found that the wear mechanisms of EH47 high-strength hull steel are an abrasive wear mechanism and a fatigue wear mechanism due to the action of sand particles and a high-loading force;

meanwhile, the micro-voids and isolated pits indicate that surface fatigue plays a great role in the wear of disks.

(2) It can be seen from the electrochemical test results of the corrosion that the corrosion product film of the experimental steel fails to better inhibit the corrosion of the matrix than the matrix itself. The results show that the corrosion of steel in a 3.5% NaCl solution is serious and that the protective effect of the corrosion product film is not obvious. At the same time, the interaction between wear and corrosion accelerates the corrosion and improves the electrochemical corrosion rate of the experimental steel.

(3) The results of the SEM, EDS and XRD analyses show that there are three main corrosion products of the experimental steel in 3.5% NaCl solution, namely, FeOOH, Fe<sub>2</sub>O<sub>3</sub>, and Fe<sub>3</sub>O<sub>4</sub>. With an extension of corrosion time, the film structure of the corrosion products changes from loose to dense.

#### ACKNOWLEDGEMENTS

The authors are very thankful for financial support from the Natural Science Foundation of China (NSFC; 1. No. 51474127: Influence of the size effect on the deformation behavior of profile and flexible rolling at the micro scale, 2. No. 51671100: Preparation of composite micro drill material and micro extrusion forming mechanism) and the State Key Laboratory of the Metal Material for Marine Equipment and Application-School of Material and Metallurgy, University of Science and Technology Liaoning co-project (No. SKLMEA-USTL 2017010 and SKLMEA-USTLN 201905).

#### References

1. G. D. Wang, Marine Engineering Steel Materials, *Chemical Industry Press*, (2017) Bei Jing, China.
2. L. Zhou, Strategic Advisory Report on the Development of Marine Engineering Materials in China, *Chemical Industry Press*, (2014) Bei Jing, China.
3. P. Henry, J. Takadoum and P. Berçot, *Corros. Sci.*, 51(2009)1308.
4. S. Mischler, *Tribol. Int.*, 41(2008)573.
5. M. Morcillo, I. Díaz and B. Chico, *Corros. Sci.*, 83(2014)6.
6. X. G. Li, Corrosion Behaviors and Mechanisms of Marine Engineering Materials, *Chemical Industry Press*, (2017) Bei Jing, China.
7. L. T. Xia, L. C. Wang and G. Q. Huang, *Chinese China Foundry Machine & Technology*, 2002(6)1.
8. J. Wang, J. Meng, X. Tang and W. Zhang, *Chinese Journal of Chinese Soci. for Corros. and Protection*, 27(2007)1.
9. H. Y. Yang and G. Q. Huang, *Chinese Corros. & Protection.*, 35(2014)576.
10. K. AL-Muhanna and K. Habib, *Desalination*, 250(2010)404.
11. L. Quej-Aké, A. Contreras and J. Aburto, *Int. J. Electrochem. Sci.*, 10(2015) 1809.
12. Y. Gao, Y. H. Sun and L. J. Sun, *Chinese Corrosion & Protection*, 39(2018) 327.
13. R. E. Melchers, *Corros. Sci.*, 81(2014)110.
14. A. Toloei, S. Atashin and M. Pakshir, *Corrosion. Reviews*, 31(2013)135.
15. S. Y. Zhang, X. Y. Cheng, L. C. Su and C. W. Jiang, *Int. J. Electrochem. Sci.*, 12(2017)2453.
16. Y. Zou, J. Wang, Y. Y. Zheng, *Corros. Sci.*, 53(2011)208.
17. Y. Y. Shen, Y. H. Dong, H. D. Li, X. T. Chang, D. S. Wang, Q. H. Li and Y. S. Yin, *Int. J. Electrochem. Sci.*, 13(2018)6310.
18. R. E. Melchers and R. Jeffrey, *Corros. Sci.*, 47(2005)1678.
19. A. Zayed, Y. Garbatov, C. Guedes Soares and G. Wang, Maritime Transportation and Exploitation of Ocean and Coastal Resources, (Eds.) C. Guedes Soares, Y. Garbatov, N. Fonseca, *Taylor &*

- Francis, 1(2015)589.
20. M. Panayotova, Y. Garbatov and C. Guedes Soares, *Proceedings of the 7th International Conference on Marine Science and Technology (Black Sea 2004)*, Union of Scientists of Varna, (2014) Varna, Bulgaria.
  21. S. Mischler, *Tribol. Int.*, 41(2008)573.
  22. A. Iwabuchi, J. W. Lee and M. Uchidate, *Wear*, 263(2007)492.
  23. A. Iwabuchi, T. Tsukamoto and Y. Tatsuyanagi, *Wear*, 156(1992)301.
  24. D. Lopez, N. A. Falleiros and A. P. Tschiptschin, *Tribol. Int.*, 44(2011)610.
  25. D. F. Moore, *The Wear of Non-Metallic Materials Mechanical Engineering Publ.*, (1978) London, England.
  26. S. W. Watson, F. J. Friedersdorf and B. W. Madsen, *Wear*, 181(1995)476.
  27. S. Akonko, D. Y. Li and M. M. Ziomek, *Tribol. Letter*, 18(2005)405.
  28. N. Papageorgiou, A. vonBonin and N. Espallargas, *Tribol. Int.*, 73(2014)177.
  29. I. Serre, N. Celati and R. M. Pradeilles Duval, *Wear*, 252(2002)711.
  30. X. Zhang, S. W. Yang and W. H. Zhang, *Corros. Sci.*, 82(2014)165.
  31. M. R. Bateni, J. A. Szpunar, X. Wang and D. Y. Li, *Wear*, 260 (2006)116.
  32. T. Balusamy and T. Nishimura, *Electrochim. Acta*, 199(2016)305.
  33. J. H. Huang, Z. G. Li and Y. H. Qian, *China Shanghai Metals*, 28(2006)6.
  34. H. Wu, J. W. Zhao, X. W. Cheng, W. Z. Xia, A. S. He, J. H. Yun, S. Q. Huang, L. Z. Wang, H. Huang, S. H. Jiao, Z. Y. Jiang, *Tribol. Int.*, 117 (2018) 24.
  35. L. C. Chen, P. Zhang, Q. Y. Xiong, P. Zhao, J. P. Xiong, Y. Zhou, *Int. J. Electrochem. Sci.*, 14 (2019) 919.
  36. M. A. Deyab, J. Taiwan. *Inst. Chem. Eng.*, 58 (2015) 536.
  37. S. S. Chen, Ambrish Singh, Yuanluqi Wang, W. Liu, K. H. Deng, Y. H. Lin, *Int. J. Electrochem. Sci.*, 12 (2017) 782.
  38. El-Sayed M. Sherif, Abdulhakim A. Almajid, *Int. J. Electrochem. Sci.*, 10 (2015) 34.
  39. Asiful H. Seikh and El-Sayed M. Sherif, *Int. J. Electrochem. Sci.*, 10 (2015) 895.
  40. Z. Y. Yong, J. Zhu, C. Qiu and Y.L. Liu, *Applied Surface Science*, 255 (2008) 1672.
  41. Y. Zhou, Q. Y. Xiong, J. P. Xiong, *Int. J. Electrochem. Sci.*, 10 (2015) 2812.
  42. T. Nickchi, A. Alfantazi, *Electrochim. Acta* 58 (2011)743.
  43. H. X. Guo, B.T. Lu, J.L. Luo, *Electrochem. Acta* 51 (2005) 315.
  44. Z. M. Gao, Changye Wang, Yangyang Liu, *Int. J. Electrochem. Sci.*, 10 (2015) 6487.
  45. El-Sayed M. Sherif and Magdy M. El Rayes, *Int. J. Electrochem. Sci.*, 10 (2015) 7493.